Research Article | Vol. 26, No. 3 | 5 Feb 2018 | OPTICS EXPRESS 3568
Optics EXPRESS

Effects of carrier injection profile on low noise thin $Al_{0.85}Ga_{0.15}As_{0.56}Sb_{0.44}$ avalanche photodiodes

LUCAS L.G. PINEL,[1] SIMON J. DIMLER,[1] XINXIN ZHOU,[1,2] SALMAN ABDULLAH,[1] SHIYONG ZHANG,[1,3] CHEE HING TAN,[1] AND JO SHIEN NG[1,*]

[1]*Department of Electronic and Electrical Engineering, University of Sheffield, Sheffield S3 7HQ, UK*
[2]*Present address: Oclaro, Caswell, Towchester, Northamptonshire, NN12 8EQ, UK*
[3]*EPSRC National Epitaxy Facility, North Campus, University of Sheffield, S3 7HQ, UK*
**j.s.ng@sheffield.ac.uk*

Abstract: Avalanche photodiodes (APDs) with thin avalanche regions have shown low excess noise characteristics and high gain-bandwidth products, so they are suited for long-haul optical communications. In this work, we investigated how carrier injection profile affects the avalanche gain and excess noise factors of $Al_{0.85}Ga_{0.15}As_{0.56}Sb_{0.44}$ (lattice-matched to InP substrates) *p-i-n* and *n-i-p* diodes with total depletion widths of 145-240 nm. Different carrier injection profiles were achieved by using light with wavelengths of 420, 543 and 633nm. For *p-i-n* diodes, shorter wavelength light produces higher avalanche gains for a given reverse bias and lower excess noise factors at a given gain, compared to longer wavelength light. Thus, using 420 nm light on the *p-i-n* diodes, corresponding to pure electron injection conditions, gave the highest gain and lowest excess noise. In *n-i-p* diodes, pure hole injection yields significantly lower gain and higher excess noise, compared to mixed carrier injection. These show that the electron ionization coefficient, α, is higher than the hole ionization coefficient, β. Using pure electron injection, excess noise factor characteristics with effective ionization ratios, k_{eff}, of 0.08-0.1 were obtained. This is significantly lower than those of InP and $In_{0.52}Al_{0.48}As$, the commonly used avalanche materials combined with $In_{0.53}Ga_{0.47}As$ absorber. The data reported in this paper is available from the ORDA digital repository (DOI: 10.15131/shef.data.5787318).

OCIS codes: (040.1345) Avalanche photodiodes (APDs); (060.4510) Optical communications.

References and links

1. L. J. J. Tan, J. S. Ng, C. H. Tan, and J. P. R. David, "Avalanche noise characteristics in submicron InP diodes," IEEE J. Quantum Electron. **44**(4), 378–382 (2008).
2. Y. L. Goh, A. R. J. Marshall, D. J. Massey, J. S. Ng, C. H. Tan, M. Hopkinson, J. P. R. David, S. K. Jones, C. C. Button, and S. M. Pinches, "Excess Avalanche Noise in $In_{0.52}Al_{0.48}As$," IEEE J. Quantum Electron. **43**(6), 503–507 (2007).
3. J. Xie, S. Xie, R. C. Tozer, and C. H. Tan, "Excess Noise Characteristics of Thin AlAsSb APDs," IEEE Trans. Electron Dev. **59**(5), 1475–1479 (2012).
4. X. Zhou, L. L. G. Pinel, S. J. Dimler, S. Zhang, J. S. Ng, and C. H. Tan, "Thin $Al_{1-x}Ga_xAs_{0.56}Sb_{0.44}$ Diodes With Low Excess Noise," IEEE J. Sel. Top. Quantum Electron. **24**(2), 3800105 (2018).
5. M. Ren, S. J. Maddox, M. E. Woodson, Y. Chen, S. R. Bank, and J. C. Campbell, "Characteristics of $Al_xIn_{1-x}As_ySb_{1-y}$ (x:0.3-0.7) Avalanche Photodiodes," J. Lightwave Technol. **35**(12), 2380–2384 (2017).
6. C. H. Tan, J. P. R. David, S. A. Plimmer, G. J. Rees, R. C. Tozer, and R. Grey, "Low Multiplication Noise Thin $Al_{0.6}Ga_{0.4}As$ Avalanche Photodiodes," IEEE Trans. Electron Dev. **48**(7), 1310–1317 (2001).
7. X. Zhou, C. H. Tan, S. Zhang, M. Moreno, S. Xie, S. Abdullah, and J. S. Ng, "Thin $Al_{1-x}Ga_xAs_{0.56}Sb_{0.44}$ Diodes with Extremely Weak Temperature Dependence of Avalanche Breakdown," R. Soc. Open Sci. **4**(5), 170071 (2017).
8. S. Xie, X. Zhou, S. Zhang, D. J. Thomson, X. Chen, G. T. Reed, J. S. Ng, and C. H. Tan, "InGaAs/AlGaAsSb Avalanche Photodiode with High Gain-Bandwidth Product," Opt. Express **24**(21), 24242–24247 (2016).

#315693 https://doi.org/10.1364/OE.26.003568
Journal © 2018 Received 22 Dec 2017; revised 16 Jan 2018; accepted 18 Jan 2018; published 1 Feb 2018

Optics EXPRESS

9. K. F. Li, D. S. Ong, J. P. R. David, G. J. Rees, R. C. Tozer, P. N. Robson, and R. Grey, "Avalanche multiplication noise characteristics in thin GaAs p^+-i-n^+ diodes," IEEE Trans. Electron Dev. **45**(10), 2102–2107 (1998).
10. K. F. Li, "Avalanche Noise in Submicron GaAs and InP Structures," PhD Thesis, University of Sheffield (1999) (Chap.4, p.78).
11. M. H. Woods, W. C. Johnson, and M. A. Lambert, "Use of a Schottky barrier to measure impact ionization coefficients in semiconductors," Solid-State Electron. **16**(3), 381–394 (1973).
12. Centronic, High Speed Detectors (BPX65). [Online].
13. Thorlabs, Fiber-Coupled LED, M420F2. (2017) [Online].
14. F. L. Schuermeyer, P. Cook, E. Martinez, and J. Tantillo, "Band-edge Alignment in Heterostructures," Appl. Phys. Lett. **55**(18), 1877–1878 (1989).
15. R. J. McIntyre, "Multiplication Noise in Uniform Avalanche Diodes," IEEE Trans. Electron Dev. **ED-1**(1), 164–168 (1966).
16. G. J. Rees and J. P. R. David, "Nonlocal impact ionization and avalanche multiplication," J. Phys. D Appl. Phys. **43**(24), 243001 (2010).
17. P. Yuan, C. C. Hansing, K. A. Anselm, C. V. Lenox, H. Nie, A. L. Holmes, B. G. Streetman, and J. C. Campbell, "Impact Ionization Characteristics of III-V Semiconductors for a Wide Range of Multiplication Region Thicknesses," IEEE J. Quantum Electron. **36**(2), 198–204 (2000).
18. C. H. Tan, J. C. Clark, J. P. R. David, G. J. Rees, S. A. Plimmer, R. C. Tozer, D. C. Herbert, D. J. Robbins, W. Y. Leong, and J. Newey, "Avalanche Noise Measurement in Thin Si p^+-i-n^+ Diodes," Appl. Phys. Lett. **76**(26), 3926–3928 (2000).

1. Introduction

Optical fiber-based communication systems typically require high bit rate and long distances between optical links. To detect weak optical signals at high bit rate, optical receivers in these systems use high-speed avalanche photodiodes (APDs). The APDs are operated to provide sufficient avalanche gain, M, which in turn increases the optical receivers' signal-to-noise ratios. The avalanche gain is the end result of successive impact ionization events taking place in the avalanche regions of the APDs.

Due to stochastic nature of impact ionization events, avalanche gain values fluctuate around a mean value, causing avalanche noise. Significant avalanche noise will negate, at least partially, if not completely, the improvement in receiver's signal-to-noise ratio brought by the avalanche gain. Hence, practical APDs must not have avalanche noise that increases rapidly with M. To characterize the avalanche noise, excess noise factors versus avalanche gain characteristics, $F(M)$, are commonly used. F tends to increase with M and its rate of increase is determined by the avalanche material, temperature, and width of the high field region, w.

The dependence of $F(M)$ characteristics on avalanche material has motivated researchers to experimentally evaluate different avalanche materials. For optical communication, narrow bandgap absorption layers, such as InGaAs, InGaAsP or InAlGaAs (grown lattice-matched to InP substrates), are combined with a wider bandgap high field region that provides the avalanche multiplication. Therefore researchers have assessed wide bandgap materials, such as InP [1], $In_{0.52}Al_{0.48}As$ [2], $AlAs_{0.56}Sb_{0.44}$ [3] and $Al_{1-x}Ga_xAs_{0.56}Sb_{0.44}$ [4] (grown lattice-matched to InP substrates), for their suitability as avalanche materials for high performance infrared APDs for optical communication. Avalanche materials lattice-matched to other substrates have also been studied, for example $In_xAl_{1-x}As_ySb_{1-y}$ [5] (GaSb substrates) and $Al_xGa_{1-x}As$ [6] (GaAs substrates).

Recently, $Al_{1-x}Ga_xAs_{0.56}Sb_{0.44}$ (x = 0.0 to 0.15) diodes with w ~110 nm were reported to have $F(M)$ characteristics better than those of InP and $In_{0.52}Al_{0.48}As$ [4]. Limited by experimental conditions, they used mixed carrier injection conditions and found that the best effective ionization coefficient ratio, k_{eff}, for the experimental $F(M)$ characteristics was ~0.1 for $Al_{1-x}Ga_xAs_{0.56}Sb_{0.44}$ (x = 0.05 to 0.15). The data indicated that electron ionization coefficient is larger than the hole ionization coefficient. Very small thermal coefficients of breakdown voltage of 0.86–1.08 $mV \cdot K^{-1}$ [7] and high gain-bandwidth products exceeding 400 GHz [8] have also been reported.

Optics EXPRESS

Based on [4], we should expect pure electron injection condition to provide the lowest possible $F(M)$ characteristics for a given w. However effects of w and carrier injection profile on $F(M)$ characteristics of $Al_{0.85}Ga_{0.15}As_{0.56}Sb_{0.44}$ (lattice-matched to InP substrates) have not been reported. In this work, we report a detailed experimental study on $Al_{0.85}Ga_{0.15}As_{0.56}Sb_{0.44}$ diodes, covering $F(M)$ data of *p-i-n* diodes under pure electron injection and *n-i-p* diodes under pure hole injection. Mixed injection conditions in *p-i-n* and *n-i-p* diodes were also covered. In addition, the study expands the range of w in comparison to previous work.

2. Experimental details

The wafers used in this work are a series of four $Al_{0.85}Ga_{0.15}As_{0.56}Sb_{0.44}$ (hereafter referred to as AlGaAsSb) diodes. They consist of two p^+-i-n^+ and two n^+-i-p^+ diodes with nominal i-region thicknesses of 100 and 200 nm. All four wafers were grown by Molecular Beam Epitaxy on semi-insulating InP substrates. Epilayer details for the *n-i-p* diode wafers are illustrated in Fig. 1(a). In each *n-i-p* diode wafer, the undoped i-region is sandwiched between a top 300 nm n-AlGaAsSb and a bottom 200 nm p-AlGaAsSb layers. Heavily doped lattice-matched $In_{0.53}Ga_{0.47}As$ top and bottom layers are deposited to achieve good ohmic contact. The *p-i-n* diode wafers have identical structures, except that the n- and p-layers are replaced with p- and n-layers, respectively.

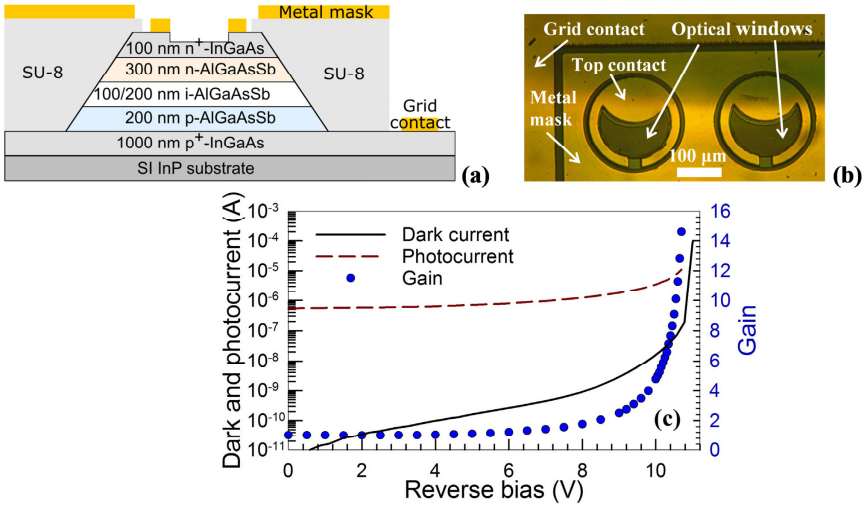

Fig. 1. Cross-sectional schematic diagram (a) and top-view photograph (b) of devices fabricated from the *n-i-p* wafers. (c) Example data of dark current, photocurrent, and deduced gain, obtained from a PIN 1 diode with a radius of 110 µm.

The wafers were fabricated into circular mesa diodes of radii 60, 110 and 210 µm using UV photolithography and wet chemical etching. The etchants used were solutions of citric acid ($C_6H_8O_7$):hydrogen peroxide (H_2O_2) in a ratio of 2:1 for InGaAs and hydrochloric acid (HCl):H_2O_2:de-ionized water in a ratio of 5:1:50 for AlGaAsSb. Ti-Au metal contacts were deposited onto the p^+ and n^+ InGaAs layers to provide ohmic contacts to the diodes. The devices were passivated using SU-8 resist (from Microchem). To prevent side injection of light that could generate an unintended mixed carrier injection profile, a layer of metal was deposited on the SU-8 covering the mesa sidewalls as illustrated in Fig. 1. This is essential when the light spot is large, such as when using an LED as the light source. Finally, to increase the collection efficiency of photo-generated carriers (and hence the photocurrent) for a given optical power of incoming light, the thickness of the top InGaAs cladding within the optical windows was reduced by etching. Examples of the fabricated devices are shown in Fig. 1(b).

Optics EXPRESS

The devices were first characterized to obtain their forward and reverse dark current versus voltage (*I-V*) characteristics. Most of the smallest diodes (60 μm radius) exhibited noticeable series resistance in their forward *I-V* characteristics, likely caused by the small top-metal contact area, so were excluded from subsequent *F*(*M*) measurements. The reverse *I-V* characteristics were used to indicate the breakdown voltage, V_b, and to select robust devices for further measurements.

Capacitance-voltage (*C-V*) measurements were then carried out on the devices selected, to provide essential data for extraction of *F*(*M*) (see below). *C-V* data from all the wafers, shown in Fig. 2(a), were also modelled (assuming a constant doping in each of the *p*-, *i*-, and *n*-layers) to estimate values of *w*. Values of *w* obtained from *C-V* modelling are compared with the corresponding nominal values for each wafer in Table 1. The calculated depletion widths at 95% of the breakdown voltage are wider than the nominal *w*, indicating some depletion into the *p*- and *n*- layers.

Table 1. Breakdown voltages, nominal *w*, and modelled *w*, capacitance at $0.95V_b$ (for 110 μm radii diodes), and depletion width at $0.95V_b$ of the four AlGaAsSb wafers.

Wafer	V_b (V)	Nominal *w* (nm)	Modelled *w* (nm)	Capacitance at $0.95V_b$ (pF)	Depletion width at $0.95V_b$ (nm)
PIN 1	11.0	100	87	23	160
PIN 2	15.9	200	170	15	240
NIP 1	10.6	100	98	26	145
NIP 2	15.9	200	193	16	225

F(*M*) measurements were performed using the setup described in [9]. The device-under-test (DUT) was illuminated by a light source, which was modulated at a frequency ~180 Hz, to produce modulated photocurrent flowing in the DUT. This photocurrent signal was converted into voltage by a transimpedance amplifier (with gain of 2200 V/A), for avalanche gain measurements. To obtain noise data, the modulated photocurrent signal was filtered by a bandpass filter (8 to 12 MHz), before being measured by a power meter to give noise power. Voltage signals from the transimpedance amplifier and the power meter were fed to lock-in amplifiers. The output of the measurement is therefore a set of photocurrent and noise signal values versus reverse bias.

The noise signal from the *F*(*M*) measurement setup can be affected by the DUT's capacitance, hence corrections were necessary to recover the real noise signal (capacitance-voltage data obtained from the DUT were utilized for these corrections). As the DUT's capacitance increases, the correction procedure becomes less reliable, resulting in a practical capacitance limit of 30 pF [10]. Data of *F*(*M*) presented here are therefore restricted to 110 μm radii diodes to satisfy the requirement. Capacitance values at $0.95V_b$ are shown in Table 1.

From the photocurrent data, *M* is given by the ratio of total photocurrent to unmultiplied primary current. The latter is estimated from values of photocurrent at low bias, i.e. before the onset of gain. Due to increased collection efficiency linked to the depletion edge movement, photocurrent does increase slightly with reverse bias before the onset of gain. This effect was accounted for using the method described by Woods *et al.* [11]. Example data (obtained from a PIN 1 diode with a radius of 110 μm) for dark current, photocurrent, and deduced *M* are plotted versus reverse bias in Fig. 1(c). Owing to absence of edge illumination (DUTs had metal masks covering the mesa sidewalls), the avalanche gain data are unaffected by edge breakdowns.

To obtain *F*(*M*), the noise data obtained from DUT were compared to shot noise measured from a Si photodiode (BPX 65, from Centronic [12]) using the same setup and light source. The light sources used in this work included two He-Ne lasers (wavelengths of 543 and 633 nm) and an LED (Thorlabs M420F2 [13], with an emission peak at 420 nm wavelength and 15 nm full width and half maximum). When used with the Si photodiode, these light sources

Optics EXPRESS

produced shot noise that increases linearly with photocurrent, as shown in Fig. 2(b). Their gradients are similar, indicating insignificant noise from the light sources, so they are appropriate for accurate measurements of avalanche noise.

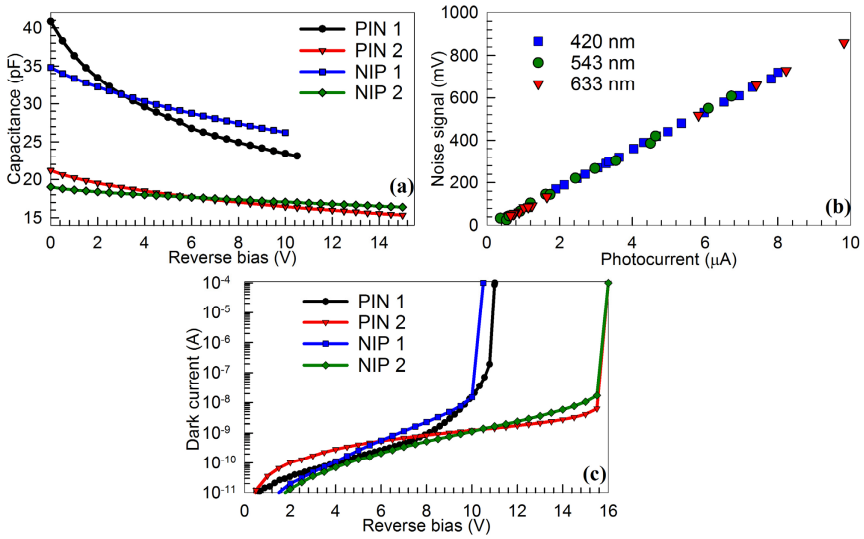

Fig. 2. (a) Capacitance-voltage data of 110 μm radii diodes of the AlGaAsSb wafers, (b) noise signal versus photocurrent of a Si photodiode measured using different light sources, and (c) dark current versus reverse bias of 110 μm radii diodes for all 4 wafers.

The different light sources were needed to generate different carrier injection profiles (pure electron, pure hole, or mixed carrier) within the diodes. To estimate the carrier injection profile for each wavelength, we estimated photon absorption coefficients at the three wavelengths for AlGaAsSb, by interpolating data from the four binary compounds, namely AlAs, AlSb, GaAs, and GaSb, as in [4]. At wavelengths of 633, 543, and 420 nm, the estimated absorption coefficients are 1.7×10^4, 5.8×10^4, and 3.0×10^5 cm^{-1}, respectively. These correspond to 39.7, 82.4, and 99.99% of the incoming light being absorbed within the top AlGaAsSb layer. The 420 nm wavelength light therefore produces pure electron injection in the *p-i-n* diodes, and pure hole injection in the *n-i-p* diodes.

Note that carriers generated by photon absorption in the top InGaAs layer are excluded from consideration. This is because large conduction and valence band offsets, such as those between InGaAs and AlAsSb [14], are likely to also exist between InGaAs and AlGaAsSb in our diodes, preventing carriers generated in the top InGaAs layer from reaching the depletion region.

3. Results and discussions

The reverse *I-V* characteristics from the four wafers, shown in Fig. 2(c), exhibit an abrupt increase in dark current, indicating dominance of avalanche breakdown. For a given wafer, the values of dark current do not scale with device area, suggesting that at low biases, surface leakage is not completely suppressed.

Data of avalanche gain versus reverse bias for all four wafers, obtained using the three different wavelengths are compared in Fig. 3. The data (taken from 3 to 6 devices per wafer per wavelength) are presented as mean values with error bars indicating the standard deviation. For a given wafer and a reverse bias, *M* increases as the illumination wavelength decreases in the *p-i-n* diodes, whereas the opposite trend is observed in the *n-i-p* diodes. In the *p-i-n* diodes, as the wavelength decreases from 633 to 420 nm, the carrier injection profile changes from mixed carrier injection to pure electron injection, producing larger *M*. This strongly indicates that the electron ionization coefficient, α, is greater than the hole ionization

Optics EXPRESS

coefficient, β, i.e. $\alpha > \beta$, consistent with [4]. We noted, in particular, that the reduction in M from mixed injection (using 543 and 633 nm), in comparison to pure hole injection (using 420 nm), is more pronounced in diodes with thicker avalanche regions.

Values of breakdown voltages are determined by extrapolating values of $1/M$ to 0, as shown in Fig. 3 (right axis), giving V_b ~11.00, 10.6, 15.9, and 15.9 V for PIN 1, NIP 1, PIN 2, and NIP 2, respectively. These breakdown voltages coincide with voltages where there are abrupt increases in the dark currents in Fig. 2(c).

$F(M)$ characteristics for all four wafers, again obtained using three wavelengths, are shown in Fig. 4. In the *p-i-n* diodes, as the wavelength decreases from 633 to 420 nm, eventually producing pure electron injection profile, the excess noise factor decreases. The opposite trend is observed in the *n-i-p* diodes. These observations indicate that $\alpha > \beta$, consistent with the data in Fig. 3 and prior work [4].

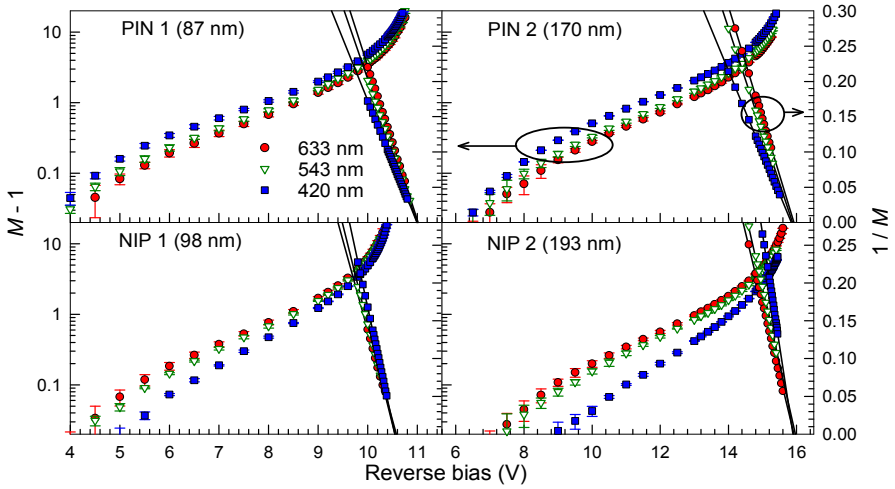

Fig. 3. Avalanche gain versus reverse bias characteristics of the four wafers, obtained using wavelengths of 633 (●), 543 (▽), and 420 nm (■). $1/M$ curves are extrapolated to zero to extract V_b.

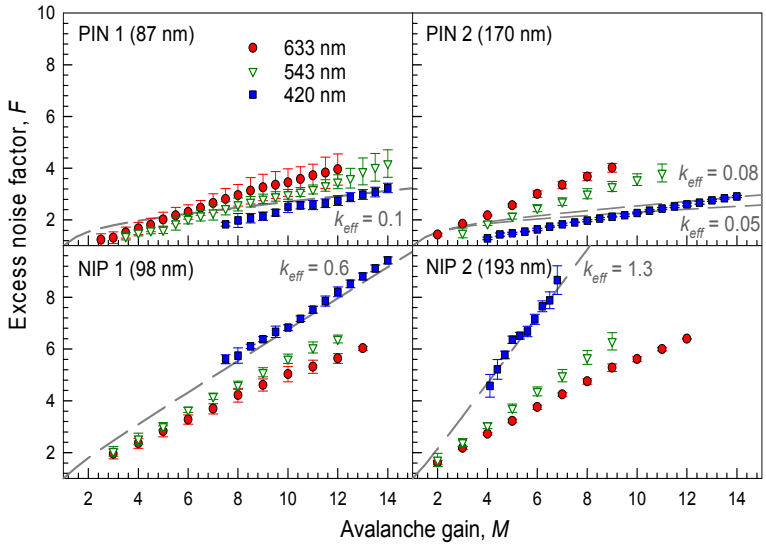

Fig. 4. Excess noise factor versus avalanche gain characteristics of the four wafers, obtained using wavelengths of 633 nm (●), 543 nm (▽), and 420 nm (■).

Optics EXPRESS

To aid comparison, data obtained using the 420 nm wavelength light (i.e. those with pure electron injection in *p-i-n* diodes and pure hole injection in *n-i-p* diodes) are fitted using the expression [15],

$$F(M) = k_{eff} M + \left(2 - \frac{1}{M}\right)\left(1 - k_{eff}\right), \quad (1)$$

where k_{eff} was used as adjustable parameter. Reasonable fits were obtained using k_{eff} of 0.1, 0.6, 0.08, and 1.3, for the PIN 1, NIP 1, PIN 2, and NIP 2, respectively. As expected from $\alpha > \beta$, the *p-i-n* diodes under pure electron injection conditions produced the smallest k_{eff} ~0.08 (best $F(M)$ characteristics). The *n-i-p* diodes exhibited much higher avalanche noise. Hence, when incorporating AlGaAsSb avalanche regions into SAM APDs, the designs should ensure pure electron injection into the avalanche regions.

Before further $F(M)$ analyses, it is worth recalling the following. The local impact ionization theory by McIntyre [15] does not include the effects of deadspace, d, which is the minimum distance traveled before a carrier achieves the ionization threshold energy to initiate an impact ionization event. When d is insignificant compared to w, $F(M)$ data obtained from pure electron injection and pure hole injection will yield k_{eff} and $1/k_{eff}$, respectively [15]. Our $F(M)$ data do not conform to this trend. For example, using 420 nm wavelength illumination on PIN 1 produced $F(M)$ data with k_{eff} = 0.1, whereas those of NIP 1 yielded k_{eff} = 0.6, much smaller than 10 (the value expected from the local impact ionization theory). This deviation is attributed to the effect of ionization deadspace in our diodes. Significant effects of non-local impact ionization (in the form of ionization deadspace) in narrow avalanche regions have been observed widely (see [16] for review).

Identifying the exact contribution of ionization deadspace to the excess noise characteristics of our AlGaAsSb diodes is beyond the scope of this work. We can nevertheless illustrate the effects of ionization deadspace on $F(M)$ data, through calculations of excess noise versus avalanche gain characteristics under pure electron and pure hole injection, $F_e(M_e)$ and $F_h(M_h)$, respectively. The $F(M)$ characteristics of hypothetical diodes with β/α = 0.5 and d/w value varying from 0 to 0.3 are compared in Fig. 5. When d/w = 0 (i.e. absence of deadspace), $F_e(M_e)$ and $F_h(M_h)$ correspond to Eq. (1) with k_{eff} of 0.5 (since β/α = 0.5) and 2.0 (inverse of 0.5), respectively. However, increasing d/w to 0.2 leads to corresponding k_{eff} values of 0.2 and 0.8, deviating significantly from 0.5 and 2.0. Further increase in d/w to 0.3 results in greater deviation from the local impact ionization theory, such that k_{eff} = 0.1 and 0.5 for $F_e(M_e)$ and $F_h(M_h)$, respectively. These k_{eff} values are close to those from the experimental results of PIN 1 and NIP 1.

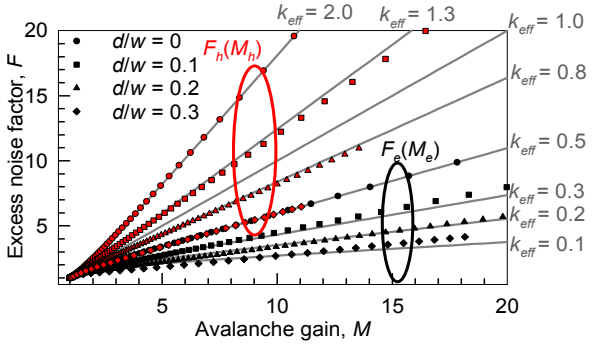

Fig. 5. Calculated characteristics of $F_e(M_e)$ (black symbols) and $F_h(M_h)$ (red symbols) β/α = 0.5. Ratios of deadspace to avalanche width used are 0, 0.1, 0.2, and 0.3.

For APD design purposes, assuming that the preferred carrier type is injected, the dependence of k_{eff} on the APD's high field region width is of great importance. As w

Optics EXPRESS

decreases, two key factors influence k_{eff} changes. These are (i) more significant ionization deadspaces (discussed above), and (ii) more similar ionization coefficients. The desirable effect of ionization deadspaces (reducing excess noise factors) is usually more pronounced in narrow APDs, because the deadspaces now occupy a larger portion of the high field region [16]. On the other hand, compared to wide APDs, narrow APDs operate at higher electric fields, where values of α and β are more similar, increasing excess noise factors.

The competing effects of (i) and (ii) lead to a local maximum for excess noise characteristics in the material InAlAs [2], as shown in Fig. 6. In InAlAs, for $w > 0.5$ μm, the excess noise increases as w decreases, because it is dominated by (ii). For $w < 0.5$ μm, (i) becomes dominant, reducing excess noise as w decreases. Our $F_e(M_e)$ data for PIN 1 and PIN 2 share the same trend, indicating that their ionization coefficients are sufficiently dissimilar. For NIP 1 and NIP 2, the consideration is simpler, because both factors serve to reduce excess noise factors, resulting in a lower k_{eff} in NIP 1 than in NIP 2. Note that when injecting the less-readily ionizing carrier type (holes in the case of AlGaAsSb), as w decreases, more similar ionization coefficients reduce excess noise. For example, assuming zero ionization deadspace, if $\alpha/\beta = 0.5$, the $F_h(M_h)$ data will yield $k_{eff} = 2.0$. As α/β approaches unity, k_{eff} will also approach unity, leading to reduced $F_h(M_h)$.

The excess noise factor values at avalanche gain ~10 from this work are compared with relevant work based on other avalanche materials in Fig. 6. These include InP, $In_{0.52}Al_{0.48}As$, and $AlAs_{0.56}Sb_{0.44}$, which are lattice-matched to InP substrates. Two other avalanche materials that exhibit low avalanche noise when sub-micron avalanche regions are used, Si and $Al_{0.3}In_{0.7}As_{0.3}Sb_{0.7}$, are also included. Care was taken to select the best possible excess noise factor for a given avalanche material, *e.g.* F_h for InP and F_e for Si. Observing Fig. 6, AlGaAsSb diodes of this work produce excess noise factors that are competitive with $AlAs_{0.56}Sb_{0.44}$ and $Al_{0.3}In_{0.7}As_{0.3}Sb_{0.7}$.

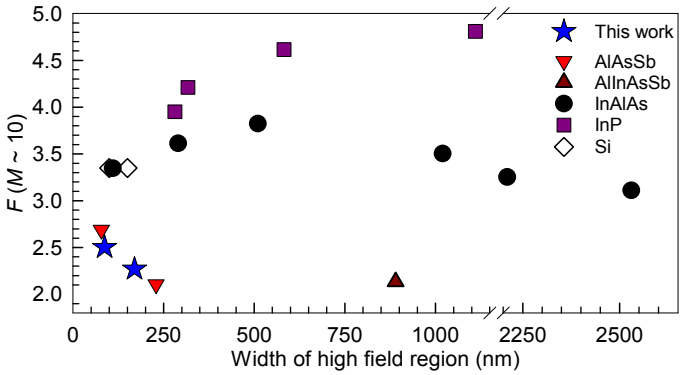

Fig. 6. Comparison of excess noise factors at avalanche gain ~10 of avalanche diodes made with AlGaAsSb (this work), AlAsSb [3], $Al_{0.3}In_{0.7}As_{0.3}Sb_{0.7}$ [5], InAlAs [2], InP [17], and Si [18].

4. Conclusion

Avalanche gain and excess noise factor were measured from a series of $Al_{0.85}Ga_{0.15}As_{0.56}Sb_{0.44}$ avalanche photodiodes with high field regions width from 87 to 193 nm. Compared to pure electron injection, mixed carrier injection produced lower avalanche gain at given reverse bias and high excess noise factor at a given avalanche gain. Hence, electrons impact ionize more readily than holes, i.e. $\alpha > \beta$, in this material. The lowest excess noise characteristic measured corresponds to k_{eff} of 0.08, lower than the best values for InP, $In_{0.52}Al_{0.48}As$, and Si. This property, along with the high achievable gain, and low dark current values, makes $Al_{0.85}Ga_{0.15}As_{0.56}Sb_{0.44}$ a suitable material to replace InP and InAlAs avalanche layers in optical communication APDs.

Optics EXPRESS

Funding

This work was supported by the UK Engineering and Physical Sciences Research Council (EP/K001469/1) and the European Union H2020 Marie Skłodowska-Curie Actions (H2020-MSCA-ITN-2014-641899).